A procedure to design toe protections against extreme through-flows for rockfill dams.

R. Morán, M.Á. Toledo, A. Larese and R. Alves.

Abstract

This article presents a procedure for designing rockfill toe protections to avoid mass sliding in dams with a highly-permeable downstream shell during extremely high through-flow episodes. This accidental through-flow may be caused by reasons such as overtopping or leakage flow due to the loss of sealing at the impervious element of the dam or its foundation. The proposed protection is located at the downstream toe of the dam and it is composed of highly permeable material, typically compacted rockfill. This material can be different from the rockfill that integrates the downstream shell of the main dam. The work is a result of a combination of a numerical and experimental research carried out to analyze the influence of the geometry of the toe protection for a given material properties of both dam shell and protection. As a result of these studies, a design methodology is obtained. A series of validation tests are presented to support the reliability of the method.

1. Introduction and background

During the last decades, a significant increment of the social demand on dam safety standards has occurred, especially in the most developed countries. This has yielded to new, and more demanding, dam regulations and technical guidelines, some of them imposing the need of protection of existing dams (EBL Kompetanse, 2005; SVENSK ENERGI, 2007). The dam protection techniques involve different adaptations of the designs of the dams to protect them against foreseeable failure mechanisms so as to increment their safety (FEMA, 2014; Lempérière, 1991).

There are different types of dam protections mainly depending on the type of dam, the associated failure mechanisms, and the requested degree of protection (Morán, 2015). In the particular case

of concrete face rockfill dams or earth-rock dams, the development of heavy through-flows within the downstream shell due to overtopping or extremely high leakages (Fig. 1) is the main cause of their partial or total failure (ICOLD, 1995). Reinforced rockfill, riprap, gabions, among others, have been the most common rockfill dam protections used in the past (Charman, Kostov, Minetti, Stoutesdijk, & Tricoli, 2001; Chinnarasri, Donjadee, & Israngkura, 2008; Fratino & Renna, 2009; Frizell, Ruff, & Mishra, 1998; ICOLD, 1993).

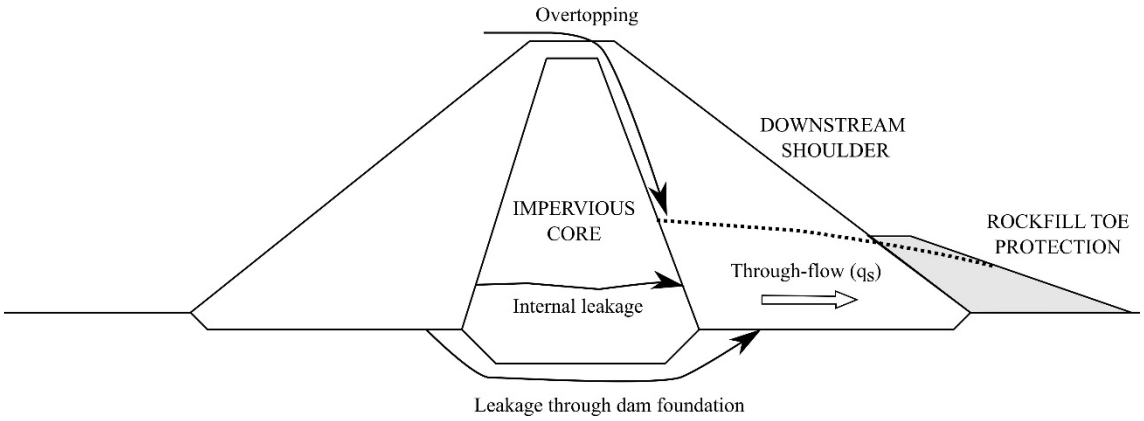

Fig. 1. Scheme of a rockfill toe protection in a preexistent dam

In addition to this, countries such as Norway or Sweden, are currently using rockfill toe protections (so-called '*rockfill toe berms*') in rockfill dams where potential for loss of life and significant downstream damages is high. This particular type of protection has been recommended by their respective National Dam Safety Guidelines to improve the stability of dams against accidental leakage (Bartsch & Nilsson, 2007; Lia, Vartdal, Skoglund, & Campos, 2013; Nilsson & Norstedt, 1998; Nilsson, 2009).

Likewise, thorough research on the mass instability caused by through-flow due to overtopping in rockfill dams has been developed during last decades (Fry et al., 2015; M. A. Toledo, 1997; M. A. Toledo, Morán, & Campos, 2012) as well as new experimentally verified numerical developments on the coupled problem of nonlinear seepage through-flow and mass slide failure of rockfill dams (A. Larese, Rossi, & Oñate, 2015; A. Larese, Rossi, & Oñate, 2011; A. Larese et al., 2011; A. Larese et al., 2013; A. Larese et al., 2013; Rossi, Larese, Dadvand, & Oñate, 2012; Rossi et al., 2012). Such research effort has made possible to deepen into the causes of the failure

47 mechanisms in rockfill dams as well as validate such numerical codes. As a result of this, it was
48 concluded that the stability of the downstream shell plays a key role to avoid severe damages in
49 the dam or its total failure (Morán, 2015; M. A. Toledo, 1998; M. A. Toledo & Morera, 2015a;
50 M. A. Toledo & Morera, 2015b). Otherwise, the downstream shell could be rapidly removed, and
51 the impervious element would lose support so as the dam breach could occur suddenly. Therefore,
52 the construction of a rockfill downstream toe, conducted to assure the stability of the downstream
53 shell, would increase significantly the safety of the existing dam.

54 According to abovementioned, the aim of the article is to present a design procedure of rockfill
55 toe protections in order to stabilize the downstream shell of the dam in extremely high through-
56 flow conditions, where unexpected pore water pressures can develop within the rockfill material.
57 This procedure was the main result of the PhD. thesis of one of the authors (Morán, 2013).

58 2. Design procedure

59 2.1. Overview

60 The procedure is applicable to preexistent rockfill dams with its downstream shell constructed in
61 rock foundations (Fig. 1). Thus, the permeability of the foundation has been neglected, assuming
62 that the through-flow seepage is developed through the downstream shell. So, under high through-
63 flow scenarios, the turbulent seepage flow is an external input that has to be estimated beforehand.
64 Such estimation of the potential discharge per unit length of the toe berm (q_s) can be done
65 considering extreme hydrologic episodes, the failure of the spillway or potential leakage flows
66 due to a failure in the impervious element of the dam, among others. The protection is designed
67 to resist through-flows within the downstream shell of the dam from inside to outside. However,
68 its behavior under external skimming flow, parallel to the downstream slope of the existing dam,
69 would not be acceptable given that the added material at the toe of the dam would perform as an
70 obstacle to such flow, which may initiate erosive processes. This condition has to be considered
71 when estimating the height of the protection as it will be shown later on. Moreover, the different
72 materials are considered as an isotropic continuum. This means that this procedure is particularly

indicated to dams with a not significantly layered rockfill material at the downstream shell. Such layering processes are especially relevant in weak rockfills due to the effect of the compaction energy of the heavy machinery and may cause a high variation of the permeability along the vertical direction.

Other input parameters for the design procedure (Fig. 2) are the downstream slope of the dam (N), the internal friction angle (φ_E) and the specific weight (γ_E) of the rockfill material of the downstream shell (E). It is widely known (Lawson, Trollope, & Parkin, 1962; Parkin, 1971) that seepage flow through high permeable continuum media implies a parabolic relation (Eq. 1) between the hydraulic gradient (i) and the average seepage velocity in the continuum (v). Therefore, in this case, the permeability of the downstream rockfill material is not linear and has to be characterized by the coefficients a_E and b_E of (Eq. 1).

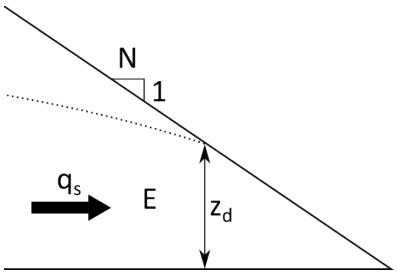

Fig. 2. Scheme of the saturation line of the seepage through-flow (q_s) at the toe of the downstream shell

$$i = a_E \cdot v + b_E \cdot v^2 \qquad \text{(Eq. 1)}$$

The output parameters of the design procedure (Fig. 3) are the length of the crest (B); the downstream slope (N_b); and the height (H_b) of the rockfill toe. The procedure assumes that the properties of the material of the rockfill toe (E_b) are known as well as those of the downstream shell (E). The properties of both materials are stated by parameters with the sub-index E (dam) and E_b (protection).

92 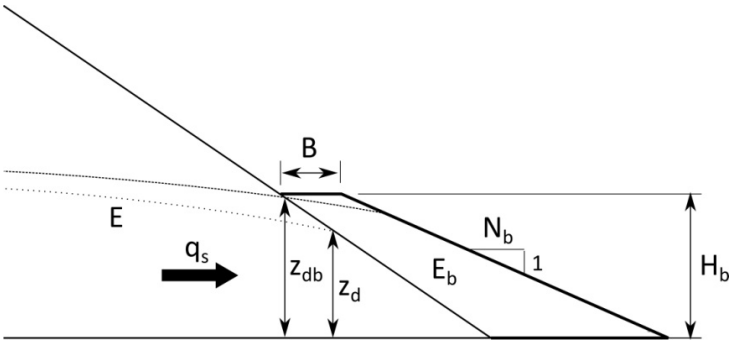

93 Fig. 3. Design parameters of a rockfill toe protection

94 Previous work by the authors concluded with design criteria for the crest length (B) and the slope
95 of the rockfill protection (N_b) to remain stable in saturated conditions (Morán & Toledo, 2011).
96 In such work, the authors stated that, for a given through-flow, the length of the crest (B) not only
97 had a minor positive effect on the mass slide stability of the dam and protection but also might
98 generate a rise of the saturation line which could be harmful for the stability of the dam. These
99 conclusions were based on a combination of experimental and numerical research. Therefore, the
100 crest length should be chosen according to construction requirements, i.e. the minimum length
101 needed for an appropriate compaction of the rockfill.

102 Additionally, Toledo obtained an expression (Eq. 2) to obtain the mass slide safety factor of the
103 rockfill slope in saturated conditions (M. A. Toledo, 1997).

$$F = \frac{1}{\gamma_{Eb,sat}} \cdot \left(\gamma_{Eb,sat} - \frac{\beta \cdot \gamma_w}{cos^2 \alpha} \right) \cdot \frac{tan\varphi_{Eb}}{tan\alpha} \qquad \text{(Eq. 2)}$$

104 where:

105 *F,* safety factor

106 β, coefficient given by:

$$\beta = -0{,}32 \cdot N_b + 1{,}52 \cdot N_b - 0{,}77; \quad if\ (1{,}5 < N_b < 2) \qquad \text{(Eq. 3)}$$

$$\beta = -0{,}32 \cdot N_b + 1{,}52 \cdot N_b - 0{,}77; \quad if\ (N_b \geq 2) \qquad \text{(Eq. 4)}$$

N_b, rockfill slope (H:V)

$\gamma_{Eb,sat}$, saturated specific weight of the material E_b

γ_w, specific weight of the water

φ_{Eb}, internal friction angle of the material E_b

α, angle between horizontal and the rockfill slope, where,

$$\tan\alpha = 1/N_b \quad \text{(Eq. 5)}$$

Consequently, applying (Eq. 2) for a given safety factor (F), the stable slope could be obtained through the value of the angle (α). This angle directly determines the slope (N_b). Given that, in most of the cases, the friction angle of the rockfill materials results in a stable slope higher than two, the coefficient β can be considered equal to one. This condition involves considering hydrostatic pore water pressure in the granular material and, therefore, the obtained result is slightly conservative. Nevertheless, if the value of the obtained slope is less than two, an iterative process could be done to consider a more accurate value of the coefficient β.

Given that this formulation (Eq. 2) was obtained numerically, a set of validation tests were developed to verify its applicability for design purposes. This validation was made for slopes greater than two, i.e., for a value of coefficient β equals one, obtaining successful results (Morán, 2013).

2.2. Estimation of the height of the rockfill toe protection

Once the length of the rockfill crest (B) and the stable slope (N_b) have been estimated according to construction requirements and (Eq. 2), respectively, the last parameter to define the rockfill protection is the protection height (H_b).

The protection height has to be high enough to avoid the development of pore water pressures in the area of the downstream shell of the dam which is not covered by the material of the rockfill toe. Otherwise, the slope of the dam would not be stable since it is usually designed in dry

conditions, i.e., in absence of pore water pressures. Such condition involves that the height of the saturation line at the contact surface between the downstream shell of the dam and the rockfill protection (z_{db}) should not exceed H_b (Fig. 3) for a given through-flow (Eq. 6).

$$z_{db} \leq H_b \quad \text{(Eq. 6)}$$

To do so, for a particular design through-flow (q_s), the height of the saturation line at the slope of the existing dam (z_d) has been considered as an additional input of the design methodology (Fig. 1). In such a way, z_d establishes a minimum value of H_b which could be finally calculated by an iterative process until the condition (Eq. 6) is fulfilled. The value of z_d can be calculated by different numerical methods, such as the open source *Kratos* [http://www.cimne.com/kratos/] (Dadvand, Rossi, & Oñate, 2010) which uses a finite element level set technique to trace the evolution of the transient seepage in variable porosity media, which assume the parabolic seepage equation using the Ergun approach (Antonia Larese, Rossi, & Oñate, 2014; A. Larese, Rossi, Oñate, & Idelsohn, 2012; A. Larese et al., 2013).

At this point, the authors have deducted a formulation to first estimation of H_b in order to complete the design procedure of the rockfill protection. The algorithm makes some conservative assumptions and simplifications which can be acceptable for design purposes, as it has been experimentally validated through a set of laboratory tests. Nevertheless, once H_b has been obtained according to this estimation, the development of a numerical seepage model of the proposed design is suggested as the final step of the design procedure.

The formulation to estimate H_b follows the basis of the research made by Toledo. In such research, it was stated that the hydraulic gradient at the toe of the rockfill has a maximum value (i_{max}) as a function of its downstream slope (N) expressed in (Eq. 7) (M. A. Toledo, 1998).

$$i_{max} = \frac{1}{N} \quad \text{(Eq. 7)}$$

Assuming the conservative hypothesis that hydraulic gradient is maximum, and constant, at the toe of the rockfill, it is possible to apply a linear seepage equation (Darcy's law), as a simplification for design purposes. Thus, a linear relationship between the maximum hydraulic

gradient (i_{max}) and the maximum seepage velocity (v_{max}) can be obtained, expressed by coefficient K_E or the linear permeability K_{dE} (Eq. 8).

$$K_E = \frac{1}{K_{dE}} = \frac{i_{max}}{v_{max}} = \frac{{}^{1}/_{N}}{\frac{-a_E + \sqrt{a_E^2 + 4 \cdot \frac{b_E}{N}}}{2 \cdot b_E}} = \frac{2 \cdot b_E}{N \cdot \left(-a_E + \sqrt{a_E^2 + 4 \cdot \frac{b_E}{N}} \right)} \quad \text{(Eq. 8)}$$

Meanwhile, H_b can be expressed as a function of z_d (Eq. 9):

$$H_b = A \cdot z_d \quad \text{(Eq. 9)}$$

Where

A is a coefficient greater or equal than 1.

Therefore, H_b could be obtained through the estimation of the coefficient A. Obviously, this coefficient must meet the condition espressed in (Eq. 6) for the particular length crest (B) and rockfill toe slope (N_b) which were fixed previously based on construction requirements and (Eq. 2).

The minimum value of H_b would be precisely z_{db} (Eq. 10) given that this would fulfill strictly the condition to avoid the development of pore water pressures in the surface of the downstream shell of the dam which is not secured by the protection material. In this case, the estimation of the coefficient A can be done through a theoretical approach assuming an equivalent linear permeability (K_{de}) in the medium defined by the rockfill protection and the toe of the covered part of the downstream shell (see the shaded area in Fig. 4) and making H_b equal to z_{db} (Eq. 10).

$$H_b = z_{db} \quad \text{(Eq. 10)}$$

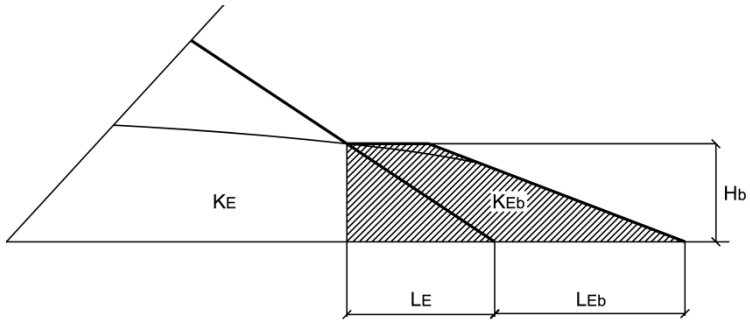

Fig. 4. Seepage area (shaded) with the imposed condition (Eq. 10)

Consequently, an equivalent permeability was theoretically deduced. As it is known (Gonzalez de Vallejo, Ferrer, Ortuño, & Oteo, 2002), the seepage through a series of j materials disposed consecutively with permeability K_{dj} and thickness L_j, in which a total hydraulic head loss (Δh) occurs, the seepage flow (Q) keeps constant within a seepage tube (Fig. 5).

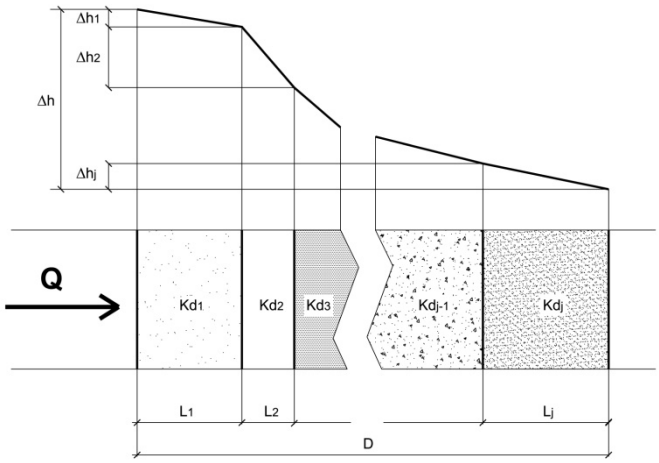

Fig. 5. One-dimensional scheme of the head losses of the seepage flow (Q) through different materials.

In such a case, the seepage flow can be expressed in terms of K_{de}:

$$v = K_{de} \cdot i_e \quad \text{(Eq. 11)}$$

Where

$$i_e = \frac{\Delta h}{\sum L_j} = \frac{\sum \Delta h_j}{\sum L_j} \quad \text{(Eq. 12)}$$

As

$$\Delta h_j = \frac{L_j \cdot v}{K_j} \quad \text{(Eq. 13)}$$

181 Then, substituting (Eq. 12) and (Eq. 13) in (Eq. 11):

$$K_{de} = \frac{v}{i_e} = \frac{v}{\frac{\sum \Delta h_j}{\sum L_j}} = \frac{v}{\frac{\sum \frac{L_j \cdot v}{K_{dj}}}{\sum L_j}} = \frac{\sum L_j}{\sum \frac{L_j}{K_{dj}}} \quad \text{(Eq. 14)}$$

182 Applying (Eq. 14) to the seepage domain defined in Fig. 4, and admitting the assumption, for
183 design purposes, that the length of the seepage path is L_E across the material (E) and L_{Eb} in the
184 material of the rockfill protection (E_b), the equivalent permeability can be obtained (Eq. 15):

$$K_{de} = \frac{L_E + L_{Eb}}{\frac{L_E}{K_{dE}} + \frac{L_{Eb}}{K_{dEb}}} = \frac{B + H_b \cdot N_b}{\frac{H_b \cdot N}{K_{dE}} + \frac{B + H_b \cdot (N_b - N)}{K_{dEb}}} = \frac{B + H_b \cdot N_b}{\frac{K_{dEb} \cdot (H_b \cdot N) + K_{dE} \cdot (B + H_b \cdot (N_b - N))}{K_{dE} \cdot K_{dEb}}} = \frac{K_{dE} \cdot K_{dEb} \cdot (B + H_b \cdot N_b)}{K_{dEb} \cdot (H_b \cdot N) + K_{dE} \cdot (B + H_b \cdot (N_b - N))} \quad \text{(Eq. 15)}$$

185 Where

186 K_{dE} represents the linear permeability of the material of the downstream shell of the dam,

187 K_{dEb} the permeability of the rockfill toe protection.

188 The average velocity at the upstream end of the seepage area (Fig. 4) can be expressed through
189 (Eq. 16):

$$v = \frac{q_s}{H_b} \quad \text{(Eq. 16)}$$

190 From (Eq. 11) and (Eq. 16), following the abovementioned assumption about the length of the
191 seepage paths:

$$\frac{q_s}{H_b} = K_{de} \cdot \frac{H_b}{L_E + L_{Eb}} \quad \text{(Eq. 17)}$$

192

193 Similarly, applying the linear seepage equation to the through-flow in the case of the seepage
194 through the material of the rockfill shell at the toe of the dam (Fig. 2) and considering the same
195 assumption for the length of the seepage path:

$$\frac{q_s}{z_d} = K_{dE} \cdot \frac{z_d}{N \cdot z_d} \quad \text{(Eq. 18)}$$

196 Matching q_s from (Eq. 17) and (Eq. 18) :

$$K_{de} \cdot \frac{H_b^2}{L_E + L_{Eb}} = K_{dE} \cdot \frac{z_d^2}{N \cdot z_d} \quad \text{(Eq. 19)}$$

197 Since:

$$L_E + L_{Eb} = B + H_b \cdot N_b \quad \text{(Eq. 20)}$$

198 Substituting and reorganizing:

$$K_{de} \cdot H_b^2 = K_{dE} \cdot \frac{B + H_b \cdot N_b}{N \cdot z_d} \cdot z_d^2 \quad \text{(Eq. 21)}$$

199 Substituting H_b in (Eq. 21) from (Eq. 9):

$$K_{de} \cdot A^2 \cdot z_d^2 = K_{dE} \cdot \frac{B + A \cdot z_d \cdot N_b}{N \cdot z_d} \cdot z_d^2 \quad \text{(Eq. 22)}$$

200 Reorganizing (Eq. 22):

$$K_{de} \cdot A^2 = K_{dE} \cdot \frac{B + A \cdot z_d \cdot N_b}{N \cdot z_d} \quad \text{(Eq. 23)}$$

201

202 Substituting H_b (Eq. 9) in K_{de} (Eq. 15) and this one in (Eq. 23):

$$\frac{K_{dE} \cdot K_{dEb} \cdot (B + z_d \cdot N_b \cdot A)}{K_{dEb} \cdot z_d \cdot N \cdot A + K_{dE} \cdot (B + z_d \cdot (N_b - N) \cdot A)} \cdot A^2 = K_{dE} \cdot \frac{B + z_d \cdot N_b \cdot A}{N \cdot z_d} \quad \text{(Eq. 24)}$$

203

204 The obtained expression (Eq. 24) is a transcendent equation where all variables have known
205 values except A, which is the unknown to be obtained by conventional numerical methods. Once
206 A is evaluated, this can be used to estimate the height of the protection (H_b) using (Eq. 9).

Appling (Eq. 24), the effect of the relation between the equivalent permeability of the materials E and E_b on the design of the protection can be analyzed. Fig. 6 shows the evolution of the coefficient A, i.e., the height of the rockfill protection, depending on the permeability ratio between the protection and dam materials (K_{dEb}/K_{dE}).

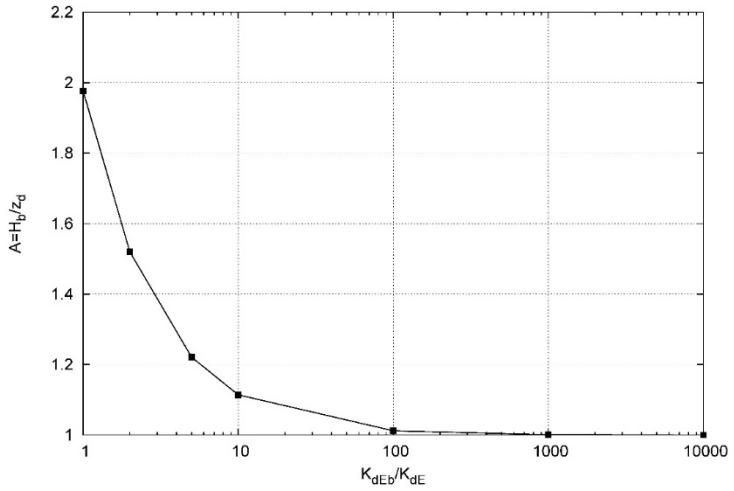

Fig. 6. Evolution of coefficient A with the permeability ratio K_{dEb}/K_{dE} (Morán, 2013)

The results show the benefit of using a high permeability ratio between materials E_b and E for the design of rockfill protection, as expected. So, as the ratio K_{dEb}/K_{dE} increases the coefficient A tends to one, which is a minimum theoretical value. Furthermore, the height of the protection exponentially increases as this ratio tends to zero. Therefore, values of K_{dEb}/K_{dE} lower than 5 should be avoided in the practice in order to get a cost-effective design.

2.3. Summary of the design procedure

In summary, the design procedure allows obtaining the parameters B, N_b and H_b, for a given unit through-flow and the features of the rockfill materials (E and E_b). Assuming all the needed data are available, the procedure follows these steps:

i. Evaluation of the length of the rockfill toe berm (B). The research studies have shown that the length of the berm has to be the minimum for an appropriate compaction of the rockfill layers during construction.

ii. Estimation of the slope of the rockfill toe (N_b) using (Eq. 2).

iii. Before obtaining the height of the protection (H_b), a seepage calculation of the downstream shell of the existing dam for the design through-flow unit discharge (q_d) is needed. The computational seepage model will be used to find the height of the saturation line at the exit in the surface of the downstream slope of the rockfill, z_d (making q_s equal to the value q_d in Fig. 2). This numerical model must consider the parabolic seepage equation (Eq. 1) of the material of the downstream shell of the existing dam (material E). With regard to this task, the authors have developed a specific numerical model which allows making these nonlinear seepage calculations (A. Larese et al., 2012).

iv. Once the value of z_d has been obtained, the protection height (H_b) can be estimated through (Eq. 9) and (Eq. 24).

v. The final design should be numerically modeled to check the fulfillment of the condition for the design through-flow (Eq. 6).

vi. Additional measures to avoid internal and external erosion should be considered by adding transition layers between the dam and protection materials or sizing the riprap layer of the external surface of the rockfill protection.

3. Experimental validation

3.1 General approach

The abovementioned design procedure was validated experimentally through a set of blind tests to verify the stability of the dam and protection. The test model was considered as the prototype for the verification, so no similarity criterion was considered necessary to validate the proposed methodology. It was assumed that the same physical phenomenon is present in the test model and in any real size prototype, and so the equations governing the mass slide will be the same as well.

In such tests, two different couples of both dam and protection materials were used. So, homogeneous gravels of sizes (D_{50}) 12.6 mm (M1), 35.0 mm (M2) and 45.0 mm (M3) were combined to design four cases of rockfill toe protection according to the new procedure. The tests were propounded in advance such that each protection was designed following the proposed

252 methodology. After the protection was dimensioned, such case was tested in the laboratory so to
253 compare the results with the theoretical behavior and, accordingly, validate or refute the
254 methodology.

255 Therefore, even though the damages caused by erosion or particle dragging were registered by
256 the instrumentation devices, they weren't considered in the analysis of the protection stability. To
257 do so, the research established criteria to distinguish between the damages caused by the two
258 predominant mechanisms of failure, either mass slide or particle dragging (Morán, 2013). This
259 analysis turned complex for unit flows near to the threshold unit-flow when particle dragging
260 initiates.

261 In addition to this, two failure tests of the unprotected dam were developed as reference cases in
262 order to be able to compare the degree of protection achieved by every rockfill toe during
263 validation. The materials used in these failure tests were M1 and M2, respectively.

264 3.2. Laboratory facility and description of the materials

265 The validation tests were performed in a 13.7 m long, 1.4 m high and 2.4 m wide channel with a
266 horizontal bottom. The channel has three functional areas (Fig.7). From upstream to downstream,
267 there is a 1 m long inlet and energy dissipation area, a 9.5 m long testing area and a 3.2 m long
268 particle catchment and sink flow area. On its right wall (in the flow direction) there is a 4.6 m
269 long and 1.1 m high glass windows for visual inspection and also for video and photographic
270 recording during the tests. In this particular test campaign, the channel width of the facility was
271 narrowed to1.32 m by adding a longitudinal internal separation wall.

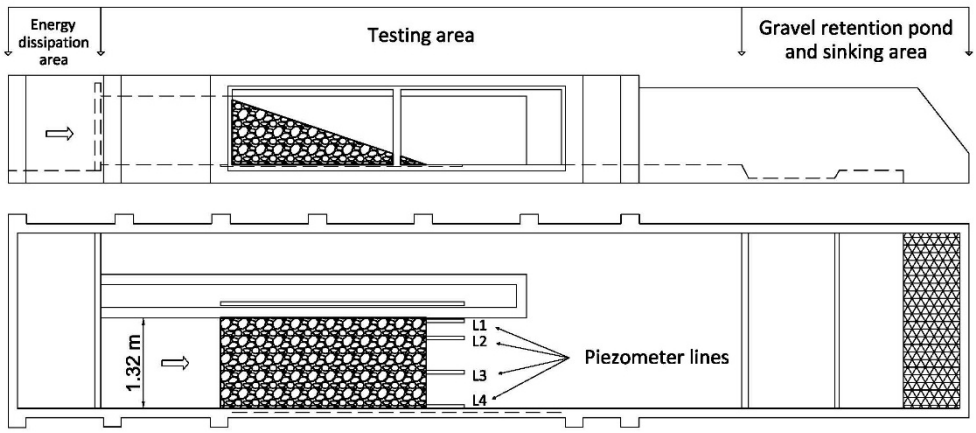

Fig.7. Side and top view of the laboratory facility

The test facility has an inlet pipe which can provide a maximum flow of 340 l/s. There is an electronically controlled valve to manage the inflows. All the testing flows were constant in each flow stage, making all the measures in steady state conditions. The main instrumentation of the tests consisted of:

- Flow measurement. Flow discharge was measured by an ultrasonic flowmeter (*Fluxus ADM 7407*). Prior to the start of the tests, the measures of the equipment were checked by the ones obtained by a discharge measurement structure consisting of a rectangular sharp crested weir at the end of the sink flow area (Fig.7).
- Water surface measurement. Three ultrasonic level meters were used, two of them installed in the testing area, upstream and downstream of the model (1 m and 8 m downstream of the inlet area, respectively).
- Digital modeling device (DMD). The DMD consists of a computer-controlled laser equipment (*SICK LMS200-30106*). Such equipment is able to measure radial distances in order to obtain a single profile of the model. The laser device is installed on a mobile frame in such a way that it is able to move along the transversal axis of the channel, obtaining as many profiles as needed to obtain the coordinates of the points of the external surface of the model. This operation is controlled automatically by a computer. The obtained coordinates of the points are moved out to a text file. Hence, this file is imported by the preprocess software GID™ to generate the mesh of the external surface of the

model (Fig. 8). Once the mesh is generated, this information can also be used for different post-process analyses as detection of modified surfaces or comparisons between relevant cross-sections.

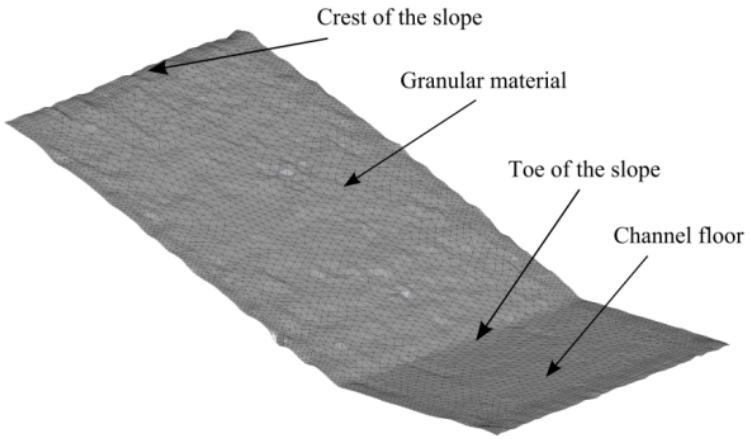

Fig. 8. Example of a generated model mesh with slope 2.6:1 (H:V) tested in the 1.32 m wide channel

The type of granular material used in the tests was limestone gravel from the same quarry, with three different grading curves (Fig. 9). Internal friction angles were determined by measuring the angle of repose of 6 samples, composed of 0.5 m high, 1.32 m long stone fills. These fills were formed by dropping the granular material. After the fill placement in dry conditions, 100 cross-section profiles, spaced every 1 cm in the middle part of the sample, were obtained by means of the DMD. Therefore, the angle of repose of each profile could be obtained. The friction angle adopted for each stone fill was the average of the repose angles of such profiles. Likewise, the friction angle of the material was the average of each stone fill. In such a way, a total of 600 cross-section profiles were considered in the analysis. In addition to this, material properties such porosity (n), uniformity coefficient (C_u), particle size (D_x) and internal friction angle (φ) were also obtained (Table 1).

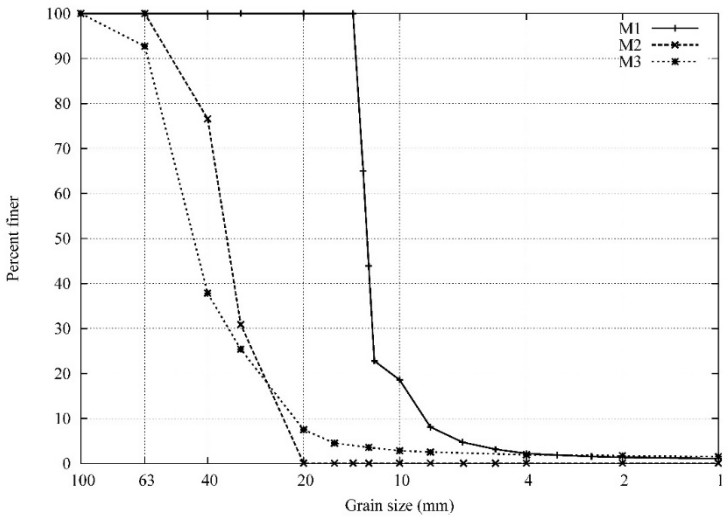

Fig. 9. Grading curves of materials used in the validation tests

Table 1. Properties of the materials used in the validation tests

Material	D_{50} (mm)	n	C_u (D_{60}/D_{10})	φ (°)	$\gamma_{e,sat}$ (KN m^{-3})
M1	12.6	0.41	1.5	36.9	19.25
M2	35.0	0.41	1.6	42.0	18.85
M3	45.5	0.41	2.3	41.7	18.98

Besides, the parabolic seepage equation (Eq. 1) of each material was calibrated through specific through-flow tests in gravel samples with a 3:1 (H:V). Hydraulic gradients and average seepage velocities were obtained from these tests (Fig. 10) using the measures of pressure heads along the base of the model (Morán, 2013).

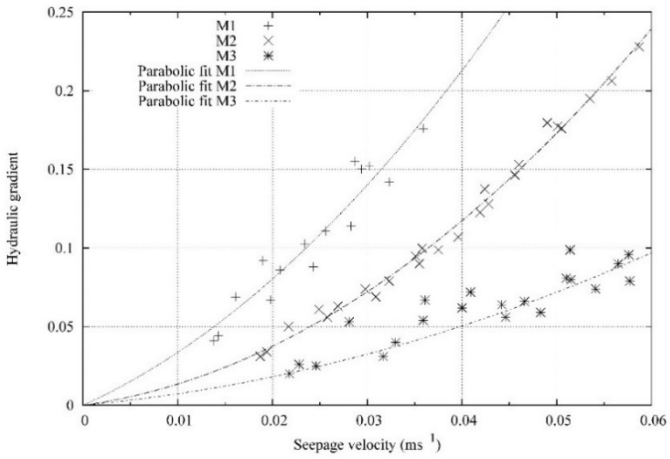

317

318 Fig. 10. Hydraulic gradients experimentally obtained for different seepage velocities and materials

319 Then, the coefficients *a*, *b* in (Eq. 2) were obtained for the three materials using a least square
320 minimization of the error of a parabolic function. Results are shown in Table 2:

321 Table 2. Results of the experimental calibration of the parabolic seepage equation of the materials used in the
322 validation tests

Material	a	b	RSS
M1	2.71	65.35	2.2×10^{-3}
M2	0.82	52.82	6.4×10^{-4}
M3	0.55	17.77	1.3×10^{-2}

323 Where

324 RSS is the sum of squares of residuals of the regression through a second-grade polynomic fit

325 3.3. Description of the validation tests

326

327 The validation tests were posed to protect two different 1 m high dam shells with slopes designed
328 according to the Spanish regulation for dams (SPANCOLD, 2015) which applies 1.4 as the mass
329 slide safety factor in normal operation. Note that this safety factor has been set considering the
330 absence of pore water pressures within the dam shell as it is usual in the dam engineering criteria.
331 The materials used for the dam shell were M1 and M2. As abovementioned, prior to the validation
332 test were done, these dams were tested to failure to be considered as the reference case. The unit

333 through-flows which caused the total failure of the unprotected dam shell (q_r) were registered to
334 be considered in the analysis of the effect of the protection. A summary of the data of the
335 validation tests is shown in Table 3.

336 Table 3. Main data of the validation tests

	Test 12_35_10	Test 12_35_16	Test 35_45_25	Test 35_45_35
Dam material, E. (D_{50} in mm)	M1 (12.6)	M1 (12.6)	M2 (35.0)	M2 (35.0)
Protection material, E_b (D_{50} in mm)	M2 (35.0)	M2 (35.0)	M3 (45.5)	M3 (45.5)
Dam height, H (cm)	100	100	100	100
Dam slope, N (H:V)	1.9	1.9	1.6	1.6
Design unit discharge of the protection, q_d (m^2s^{-1})	0.010	0.016	0.025	0.035
Unit discharge causing the failure of the unprotected dam, q_r (m^2s^{-1})	0.020	0.020	0.034	0.034
q_d/q_r ratio	0.50	0.80	0.73	1.02

337 Consequently, considering the data of each validation test (Table 3), the correspondent rockfill
338 toe protections were defined by applying the proposed design methodology (Table 4). In these
339 cases, the criterion to stablish the length of the berm (B) was to be four times the size D_{50} of the
340 protection material.

341 Next, the toe protections were prepared at the lab and tested for different through-flow discharges
342 to verify the methodology. The effect of the protection was evaluated through the *maximum*
343 *advance of the damage* (B_c), measured from the position of the downstream toe of the rockfill at
344 the beginning of the test, in the longitudinal direction of the channel. This length can be expressed
345 with the dimensionless ratio B_c/L, being L the horizontal distance between the toe and the
346 downstream end of the crest of the dam shell (Fig. 11). Accordingly, L_A is the horizontal distance
347 between the downstream toe and the point A, which is the intersection between the berm crest
348 and the slope of the dam shell. Thus, when B_c exceeds L_A, the dam begins to be damaged by the
349 through-flow. The protection is considered successful if the dam is not harmed for the design unit
350 discharge (q_d), i.e. when B_c is lower than L_A with such discharge.

Table 4. Dimensions of the rockfill toe protections corresponding to the validation tests

	Test 12_35_10	Test 12_35_16	Test 35_45_25	Test 35_45_35
Berm length, B (cm)	14	14	18	18
Rockfill toe slope N_b (H:V)	2.9	2.9	2.8	2.8
Rockfill toe height, H_b (cm)	28	40	47	59
L_A/L	0.41	0.53	0.64	0.74

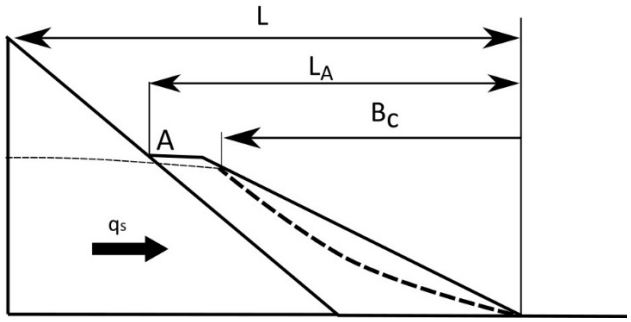

Fig. 11. Definition scheme of the maximum advance of the breakage (B_c)

3.4. Results of the validation tests

The results of the tests are shown in Fig. 12. Each data series represents the *failure paths* (Miguel Á Toledo, Campos, Lara, & Cobo, 2015) of both the unprotected and protected dam shell. Such failure path shows the evolution of the dimensionless maximum advance of the damage (B_c/L) for different unit through-flow discharges (q_s) registered at each test. In abscises, such unit through-flow discharge is represented as a dimensionless parameter referred to the unit flow which causes the total failure of the unprotected dam (q_r). The results of B_c were measured independently of the prevailing mechanism of failure. However, as the flow discharge was necessarily increasing, the dragging of particles was predominant in relation to mass slide for higher unit discharges, as expected. Fig. 12.a) shows the evolution of the failure of the protections 12_35_10 and 12_35_16 for the design unit discharge of 50% (0.010 m^2s^{-1}) and 80% (0.016 m^2s^{-1})

of the unit discharge which caused the failure of the unprotected dam, respectively. Similarly, Fig. 12.b) shows the evolution of the failure of the protections 35_45_25 and 35_45_35 for the design unit discharge of 73% (0.025 m^2s^{-1}) and 102% (0.035 m^2s^{-1}) of the failure unit discharge of the unprotected dam, respectively. Note that, in Fig. 12, the rockfill protection extends from the toe (0 in the axis B_c/L) to the point A (L_A/L in the same axis) for each validation case. Therefore, the damages affect the material of the protected dam since the moment that failure path surpasses such point.

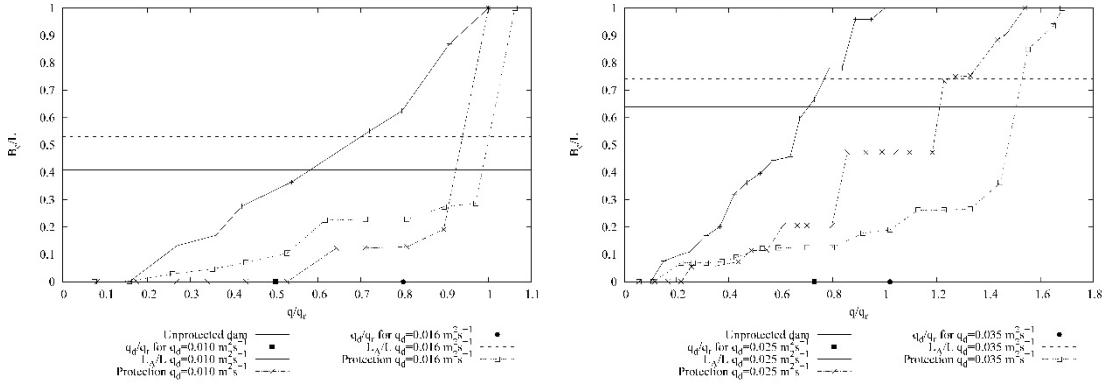

a) b)

Fig. 12. Failure paths obtained from of the validation tests.

a) Cases 12_35_10 and 12_35_16. b) Tests 35_45_25 and 35_45_35

3.5. Discussion of the validation

The results of the tests showed that protection increased the stability of the dam. Particularly, for the design unit discharge (see example in Fig. 13) the dam was not harmed, as expected. Furthermore, the damages observed for higher unit discharges were caused mainly by dragging of particles and the conclusions of the tests indicated that the effect of the protection remained even for unit discharges higher than the design value.

a)

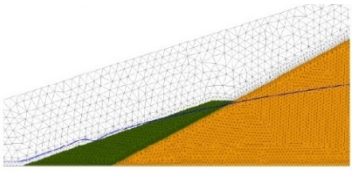

b) c)

Fig. 13. Test 12_35_16. a) Photo showing the damage in the dam without any protection for q_d. b) numerical model of the same through-flow with the proposed protection. c) Photo of the correspondent validation test.

The failure paths (Fig. 12) show the achieved degree of protection through the difference of the maximum breakage (B_c/L) of both unprotected (reference case) and protected dam. The protection effect continued even for through flows higher than q_d. Thus, in the 12_35 tests (Fig. 12. Left), the dimensionless design unit through-flows (q_d/q_r) were 0.5 and 0.8. However, for a value of 0.9, higher than the design values in both cases, the protection achieved an important degree of protection, as can be checked in Fig. 12, through the difference of the B_c/L values and the ones correspondent to the case of the unprotected dam. Thereby, the damages on the protected dam were limited to values between 20% and 30% while the unprotected dam was harmed approximately on the 85% of its height. This fact was more outstanding in the 35_45 tests, where the protected dam increased the value of the unit discharge which produced the total failure (B_c/L equal to one), between 50 to 70% regarding the unit discharge which made the unprotected dam fail, i.e. q_d/q_r equal to one. This improvement of the performance of the protection even for unit discharges higher than q_d involves an additional benefit of this kind of protection. In conclusion, the obtained results validated the proposed methodology.

406 Additionally, it was concluded that the performance of the protection may be increased by a
407 specific treatment of the external surface of the rockfill so as to avoid the dragging of stones at
408 the outer surface. This can be done through a rockfill layer with specific sizing to avoid particle
409 dragging for specific unit discharge (Hiller, 2017; Lia et al., 2013) or other techniques (ICOLD,
410 1993). It seems this complement could increase the degree of protection significantly, with a low
411 extra cost, as it was noted on the tests where the effect of the dragging of particles was reduced.

412

413 ## 4. Summary and conclusions

414 A new design methodology for rockfill toe protections to ensure the mass slide stability of dams
415 with a highly permeable downstream shell during accidental through-flow processes has been
416 presented. Such processes can be caused by overtopping or extreme internal leakage which are
417 the main causes of embankment dam failures. The proposed methodology has been
418 experimentally validated through laboratory tests. Furthermore, a future research line focused on
419 external reinforcement against particle dragging applied to this kind of protection has been
420 proposed in order to increase its performance.

421 ## Acknowledgements

422 This research was developed with funds from the Spanish National Research and Development
423 Program (2008-2011) through the research project titled ”*Rotura del elemento impermeable de*
424 *presas de materiales sueltos en situación de sobrevertido y análisis de protecciones combinando*
425 *modelación física e inteligencia artificial*”, with ID code BIA2010-21350-C03-03. The authors
426 also gratefully acknowledge the help of Prof. Eugenio Oñate, Dr. Fernando Salazar, and Dr.
427 Riccardo Rossi.